Isomer-Selective Study of the OH Initiated Oxidation of Isoprene in the Presence of O-2 and NO. I. The Minor Inner OH-Addition Channel

ARTICLE *in* THE JOURNAL OF PHYSICAL CHEMISTRY A · NOVEMBER 2009

Impact Factor: 2.69 · DOI: 10.1021/jp908543a · Source: PubMed

Isomer-Selective Study of the OH Initiated Oxidation of Isoprene in the Presence of O_2 and NO. I. The Minor Inner OH-Addition Channel

Erin E. Greenwald,[†] Buddhadeb Ghosh,[†] Katie C. Anderson,[†] Kristin S. Dooley,[†] Peng Zou,[‡] Talitha Selby,[‡] David L. Osborn,[‡] Giovanni Meloni,[‡,§] Craig A. Taatjes,[‡] Fabien Goulay,[‡,||] and Simon W. North*,[†]

Department of Chemistry, Texas A&M University, P.O. Box 30012, College Station, Texas 77842, Combustion Research Facility, Mail Stop 9055, Sandia National Laboratories, Livermore, California 94551-0969, Department of Chemistry, University of San Francisco, 2130 Fulton Street, San Francisco, California 94117, and Department of Chemistry, University of California, Berkeley, Berkeley, California 94720

Received: September 3, 2009; Revised Manuscript Received: October 12, 2009

We report isomer-selective kinetics and mechanistic details for the hydroxyl radical-initiated oxidation of isoprene, in the presence of O_2 and NO, employing complementary experimental and theoretical techniques. Using a recently demonstrated photolytic route to initiate isomer-selective kinetics in OH-initiated oxidation of unsaturated hydrocarbons via the UV photolysis of iodohydrins, the photolysis of 1-iodo-2-methyl-3-buten-2-ol results in a single isomer of the possible four OH-isoprene adducts, specifically the minor channel associated with OH addition to one of the inner carbon atoms. Employing both the laser-photolysis/laser-induced fluorescence (LP/LIF) technique and time-dependent multiplexed photoionization mass spectrometry, we find clear experimental evidence supporting the prompt rearrangement of the initially formed β-hydroxyalkyl radicals to α-hydroxyalkyl radicals, in agreement with Rice−Ramsperger−Kassel−Marcus (RRKM)/master equation predictions. We have determined a rate constant of $(3.3 \pm 0.5) \times 10^{-11}$ cm^3 molecule^{-1} s^{-1} for molecular oxygen to abstract a hydrogen atom from the α-hydroxyalkyl radical to form 4-penten-2-one and HO_2. This reaction provides a mechanistic route to C_5 carbonyl species as first-generation end products for the addition of hydroxyl radical to isoprene in the presence of O_2 and NO.

Introduction

Isoprene is the dominant nonmethane organic compound emitted to the atmosphere, and the combination of a high emission rate (500 Tg yr^{-1}) with high reactivity make understanding its fate central to modeling regional and global atmospheric processes.[1−3] The OH-initiated oxidation of isoprene results in the production of tropospheric ozone[4,5] and secondary aerosols.[6]

One of the difficulties in studying the oxidation of isoprene is the intrinsic number of isomeric species. The addition of OH radical to isoprene results in four distinct hydroxyalkyl radicals as shown in Scheme 1.

Such complexity, shown above for only the initial reaction step, has proved challenging to unravel despite the numerous studies on the detailed mechanism of isoprene oxidation. There is lack of direct experimental measurements of the intermediate branching ratios which give rise to specific isomers, each leading to final products. Thus, such information is critical to the development of chemical mechanisms in order to connect isoprene to specific first generation end products. In addition, although there is consensus that methyl vinyl ketone, methacrolein and formaldehyde are the major first-generation end products, there is still uncertainty regarding the chemical identity of minor end products. Ab initio studies have made progress in providing a priori predictions of branching ratios in isoprene oxidation. Recently a two-transition-state model has been applied to the prediction of the isomeric branching in the addition of hydroxyl radical to isoprene.[7] The two-transition model treatment was based on previous work on the OH + C_2H_4 reaction which was able to reproduce experimental results to within 10% over the temperature range of 10 to 600 K.[8] In the case of OH + isoprene a 300 K branching ratio of 0.67:0.02:0.02:0.29 was determined for formation of the four possible OH-isoprene adduct isomers, I:II:III:IV, and was found to be relatively insensitive to temperature.[7] Theory has also been valuable in identifying oxidation products but experimental confirmation of many aspects of the oxidation mechanism is as yet unavailable. To date, laboratory kinetics studies of isoprene oxidation have been limited to nonisomer-specific measurements. Although such "lumped kinetics" studies can provide useful information on the overall kinetics of the dominant species,

SCHEME 1

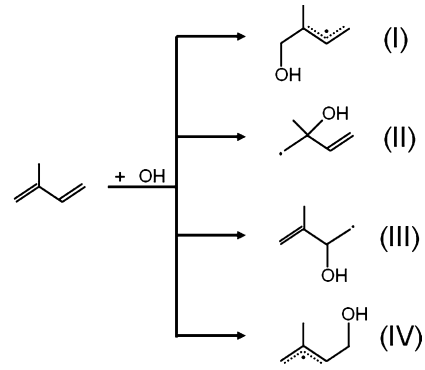

* Corresponding author.
[†] Texas A&M University.
[‡] Sandia National Laboratories.
[§] University of San Francisco.
[||] University of California, Berkeley.

10.1021/jp908543a CCC: $40.75

subtle details of the oxidation mechanism are often obscured. This is particularly true for the minor pathways associated with OH addition to the inner carbons where new cyclic isomerization routes have been predicted by theory.

We have recently demonstrated a photolytic route to initiate isomer-selective kinetics in OH-initiated oxidation of unsaturated hydrocarbons using the UV photolysis of iodohydrins. Specifically, we reported on the fate of nascent β-hydroxyalkyl radicals formed when 1,3-butadiene undergoes oxidation by hydroxyl radical addition via electrophilic addition to the inner carbons. Addition reactions result in chemically activated adducts, and the fate of these adducts is dependent on their internal energy. We have shown that measuring the iodine atom kinetic energy arising from the photolysis of the iodohydrin precursor using velocity map ion imaging permits direct determination of the internal energy distribution of the nascent adduct radical, ensuring that the energy distribution mimics electrophilic-OH addition. Theory predicts a substantial fraction of the β-hydroxyalkyl radicals should isomerize to α-hydroxyalkyl radicals prior to collisional relaxation and that the fate of the α-hydroxyalkyl radicals is reaction with O_2 by hydrogen abstraction to yield C5 carbonyls. The time-dependent production of OH following iodohydrin photolysis (in the presence of NO), detected using laser-induced fluorescence, was consistent with the cyclic isomerization mechanism and subsequent reaction of the α-hydroxyalkyl radicals.

In the present study, we report on kinetics of isomer-selective chemistry of isoprene. The study combines several experimental techniques. Ion imaging experiments are employed to characterize the photolytic preparation of isomer II (III) as well as its nascent energy distribution. The energetics of the isomerization reaction have been evaluated using quantum-chemical calculations, and the final branching ratios between the β-hydroxy and α-hydroxy radicals are determined using RRKM theory coupled with the master equation formalism. Finally, the kinetics of OH formation in the presence of O_2 and NO has been studied using both multiplexed photoionization mass spectrometry and the laser photolysis/laser induced fluorescence technique (LP/LIF) technique. The results confirm a significant yield of α-hydroxy radicals and provide a 298 K rate constant for the α-hydroxy radical reaction with O_2. This study represents the first report of isomer-selective kinetic studies of the OH initiated oxidation of isoprene and demonstrates important new chemistry for the inner OH-addition products.

Experimental Section

The velocity-map ion-imaging apparatus has been described in detail elsewhere.[9] A pulsed molecular beam of 1% iodohydrin in He (1 atm) was collimated by a conical skimmer and crossed at 90° by the focused output of two tunable pulsed laser beams. A 248 nm photolysis beam was copropagated with the probe beam near 304 nm for state-selective ionization of the iodine atom fragments using 2 + 1 REMPI (304.6 nm for $I(^2P_{3/2})$, hereafter notated as I and 303.9 nm for $I(^2P_{1/2})$, hereafter notated as I*). The 248 nm light was generated by doubling the output of an ND:YAG (Spectra-Physics Lab 150−10) pulsed dye laser (PDL) running DCM and mixing with the 1064 nm fundamental of the YAG. The light near 304 was generated by doubling the output of an ND:YAG (Spectra-Physics Lab-150−10) pumped dye laser (LAS) running a mixture of Rhodamine-640 and Rhodamine-610. The resulting ions were accelerated the length of a 50 cm flight tube using ion optics and detected by a 40 mm diameter dual microchannel plate (MCP) coupled to a phosphor screen assembly. The MCP plates were gated to collect only $m/z = 127$. Images were collected with a fast scan charge-coupled device camera and integrated using a data acquisition system. A PMT assembly was used to measure ion arrival times in order to elect the timing-gate of the MCP.

The details of the multiplexed time-resolved mass spectrometry kinetics apparatus are presented elsewhere,[10−13] and here we provide only a brief summary. A 248 nm pulsed photolysis laser beam (4 Hz) from an excimer laser coaxially irradiated a 0.6 m quartz reactor where iodohydrin and oxygen were mixed and buffered to 4 Torr total pressure in He. The system was operated under slow-flow conditions, where the gas in the reactor tube was replenished between photolysis pulses, but quasi-static on the time scale of the reactions. A typical flow velocity was approximately 4 m/s. A pinhole in the reactor tube wall allowed sampling of gas-phase reaction products into the relatively high-vacuum source region of the chamber. Typical pressures in this region were on the order of 10^{-5} Torr. The product molecules were then collimated through a conical skimmer into an ionization region, where they were crossed by a tunable VUV radiation from the synchrotron light source at the Advanced Light Source at Lawrence Berkeley National Laboratory. The resulting ions from VUV ionization were then accelerated by a series of ion optics and separated by mass using a 0.9 T magnet. Single ion counts of all masses in coincidence were then detected by a time and position sensitive mass spectrometer in the high vacuum region of the chamber (10^{-9} Torr).[10]

The LP/LIF has also been discussed in detail elsewhere.[14] The 248 nm photolysis beam from an excimer laser (EX10 GAM laser) was collinearly aligned through the reaction cell with a probe beam generated using a KDP crystal to double the output of a pulsed dye laser (Quantel TDL-51) running Rhodamine 590 or Rhodamine 610 dye pumped by the 532 nm second harmonic from an Nd:YAG laser (Spectra Physics Quanta Ray INDI). The OH radical concentration was monitored using the LIF technique to monitor OH exciting on the $Q_1(1)$ transition of the $A \leftarrow X$ (1,0) vibrational band near 282 nm. The resulting $A \rightarrow X$ (1,1) fluorescence at 308 nm was collected with a lens/filter assembly, detected by a photomultiplier tube (PMT), and integrated using a digital oscilloscope. The delay between photolysis and probe laser pulses was controlled by a digital delay/pulse generator (Stanford Research System, DG 535). Each fluorescence decay was typically averaged over 80−100 shots and followed for at least 300 μs. Argon was flowed through a bubbler containing the precursor iodohydrin molecule and introduced into the cell through a flow meter. The NO (Sigma Aldrich, 98.5%) was flowed through an ascarite trap and a bulb of known concentration was prepared with an argon buffer. O_2 (BOTCO, 99.995%) was also buffered with argon (BOTCO) to make a bulb of known concentration. Experiments were run at fixed concentration of iodohydrin, while varying the concentration of NO and O_2. The total pressure of the reaction cell was always buffered to (50 ± 4) Torr in Argon.

The synthesis of the 1-iodo-2-methyl-3-buten-2-ol was based on the synthetic preparation by Barluenga and co-workers.[15] Since the present synthesis was not explicitly presented in that work, we summarize the relevant steps (Figure 1). Briefly, 14.8 g of sodium iodide (98.9 mmol, EM Science, 99.5%) was added to a mixture of 25 mL of distilled water and 120 mL of tetrahydrofuran (THF; EMD Chemicals, GR ACS). The solution was stirred rapidly in an ice bath until the reaction flask cooled to 0 °C. An excess of 15 mL of isoprene (150 mmol, Alfa Aesar, 99%) was added to the reaction flask. Next, 83 mL of sulfuric acid[16] (7.2 M, Em Chemicals, 95−98.0%) and 33 mL of 30%

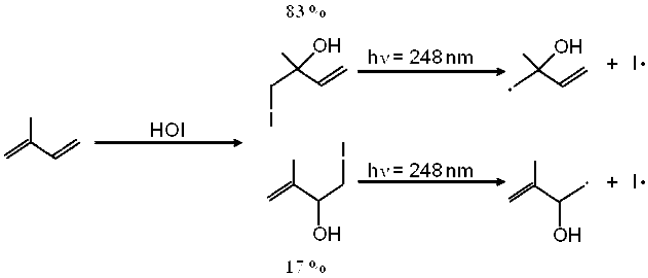

Figure 1. Synthetic preparation of a photolytic precursor corresponding to isomer II (83%), with a minor yield (17%) of a photolytic precursor corresponding to isomer III.

hydrogen peroxide (Em Science, 30% solution) were added dropwise. The reaction flask was stirred for 8−12 h while the ice bath was allowed to melt. The reaction was then quenched with 300 mL of 5% sodium thiosulfate solution (Mallinckrodt, AR). THF was removed via distillation under vacuum, and the remaining solution was extracted in 3 times with 75 mL of diethyl ether (EMD Chemicals) and washed with brine solution. The ether was removed via distillation under vacuum. Typically, the product was purified via flash column chromatography in diethyl ether to remove polymer formed throughout the reaction process. Several attempts were made to separate out the minor product (the iodohydrin corresponding to isomer 3, which was formed with a yield of approximately 17%) via column chromatography. A variety of solvent mixtures were tested using thin layer chromatography including 15% ethanol in hexanes, 20% ethanol in hexanes, pure ethanol, pure hexanes, 5% ether in hexanes, 10% ether in hexanes, 25% ether in hexanes, 50% ether in hexanes, along with variations of the prescribed separations outlined by Barluenga et al.[15] We found that even though multiple spots were seen on TLC plates, in practice, during the fractional collection, no separation was achieved.[17] The final product, after the flash column chromatography step, was distilled under vacuum to remove the ether.[18]

Product characterization was achieved via ^{1}H NMR. The ^{1}H NMR spectrum is provided in the Supporting Information. Further evidence of the constitutionality of the product is evidenced in the mass spectra (vide infra). The UV/vis absorption spectrum of the iodohydrin is also provided in the Supporting Information.

Results and Discussion

Molecular Beam Ion Imaging. The hydroxyalkyl radicals formed via OH addition to isoprene in the atmosphere have an internal energy distribution consistent with chemical activation. The internal energy distribution is reasonably described by a Boltzmann distribution of energy characterized by the ambient temperature and shifted by the exothermicity of the reaction. This internal energy distribution provides the nascent β-hydroxyalkyl radicals with sufficient internal energy to ensure that cyclic isomerization to form α-hydroxyalkyl radicals is competitive with collisional relaxation. The reaction of the β-hydroxyalkyl radicals with O_2, to form peroxy radicals, however, is considerably slower than isomerization. Therefore, kinetics measurements which aim to assess reactions under atmospheric conditions must be initiated with an ensemble of radicals whose internal energy mimics that of chemical activation. Careful determination of the internal energy distribution of the nascent radicals formed via photolysis provides requisite information for the interpretation of the subsequent kinetics. Raw photofragment images are shown in the left panels of Figure 2. The

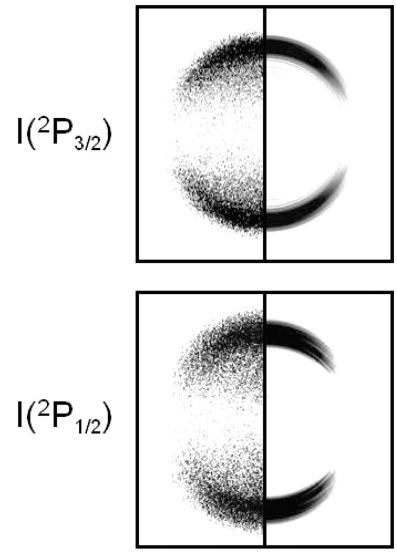

Figure 2. Raw (left) and reconstructed (right) photofragment images of the ground state ($^2P_{3/2}$) and excited state ($^2P_{1/2}$) iodine atoms formed upon photolysis of the iodohydrin photolytic precursor.

electric field vector of the laser is vertical in the plane of the image. The images represent 2D projections of the 3D velocity distributions. Conversion of the raw images into speed and angular distributions was achieved using the basis set expansion program (pBasex) for image reconstruction.[19] The reconstructed images are shown in the right panels of Figure 2. The photofragment angular distributions can be described by the form[20]

$$P(\theta) \propto \frac{1}{4\pi}[1 + \beta P_2(\cos\theta)] \quad (1)$$

where β is the spatial anisotropy parameter and $P_2(\cos\theta)$ is the second Legendre polynomial. We have determined a best fit speed-independent anisotropy parameter of $\beta = 1.9 \pm 0.2$ for the case of 1-iodo-2-methyl-3-buten-2-ol for both channels, consistent with a parallel transition to a repulsive excited state potential.

The *I*/*I** branching ratio was determined by integration of the Doppler profiles for the *I*/*I** transitions using identical laser power. The integrated Doppler profiles were corrected using the relative 2 + 1 REMPI detection efficiencies of *I* and *I**.[21] Independent confirmation of the detection efficiencies was obtained using the photodissociation of CH_3I at 266 nm. On the basis of this analysis, we determine that the yields of *I* and *I** products are approximately equivalent. This is in contrast to our previous studies of the analogous iodohydrin derived from 1,3-butadiene where we observed almost exclusive production of *I** for photodissociation at 266 and 248 nm.[22] The energy partitioning and *I*/*I** branching ratio are very similar to the results of previous alkyl iodide photolysis near 260 nm[23] and notably to the recent example of iodohydrin photodissociation.[22] The speed distribution of the iodine fragment provides a measure of the C_5H_8OH radical fragment internal energy through linear momentum and energy conservation. The internal energy distribution of the unseen fragments formed in coincidence with either *I* or *I** is determined by

$$E_{\text{avail}} = h\nu - D_0^0(C-I) = E_{\text{Trans}} + E_{\text{SO}}(I) + E_{\text{R,V}}(C_5H_8OH)$$

where D_0^0(C−I) is the C−I bond dissociation energy (55.4 kcal/mol),[24] E_{SO}(I) is the iodine spin−orbit energy, and $E_{R,V}(C_5H_8OH)$

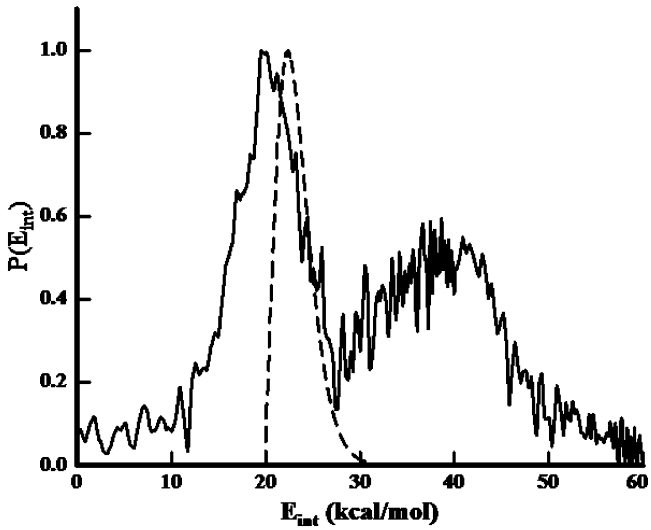

Figure 3. Internal energy distribution of the nascent β-hydroxyalkyl radicals formed in coincidence with ground and excited state iodine atoms upon the photolysis of the iodohydrin precursor measured by VELMI (solid lines) overlaid with the Boltzmann distribution of energies (dashed line), shifted by the exothermicity of the reaction for the OH addition to the second position of isoprene.

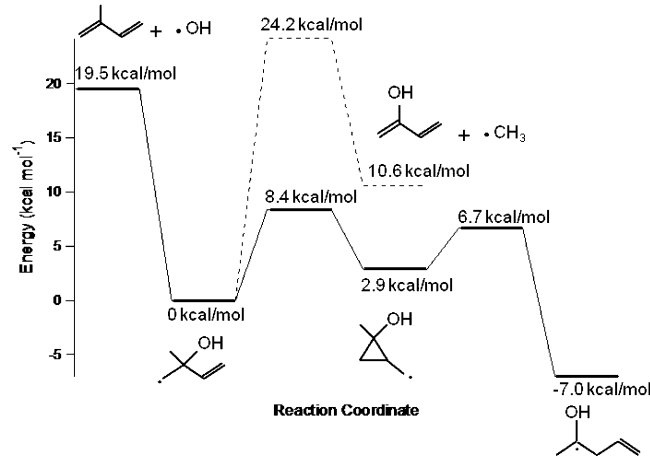

Figure 4. Schematic reaction coordinate associated with isomerization and fragmentation of the nascent β-hydroxyalkyl radicals.

is the rovibrational energy content of the β-hydroxyalkyl radical. The larger velocity of the *I* atoms reflects the additional translational energy available to the fragments as compared to the *I**, where a fraction of the available energy is bound as electronic excitation of the iodine atom. The final C_5H_8OH internal energy distribution, representing weighted averages of the *I* and *I** components, is shown in Figure 3 (solid line). The two peaks evident in the distribution correspond to radicals formed in coincidence with the two spin−orbit states of the iodine coproduct. The dashed line corresponds to the 300 K Boltzmann distribution of energies shifted by the exothermicity of the OH addition to isoprene (19.5 kcal/mol) as calculated at the B3LYP/6-311++G** level of theory. The significant fraction of radicals associated with the higher energy maximum undergo prompt dissociation (vide infra) to form isoprene and OH, leaving only the radicals associated with the lower energy feature to subsequently react.

In order to confirm the relevance to atmospheric reactivity and to assist in analysis of kinetics data, we modeled the fate of the nascent β-hydroxyalkyl radicals using the RRKM/ME formalism. The modeling employed here was similar to that discussed by Park et al.[25] and Greenwald et al.[7] Quantum chemical calculations using the Gaussian 03[26] software package were performed to provide all relevant energetics, geometries, and frequencies to obtain state counts as a function of energy for the OH-isoprene radical cyclic isomerization reaction. The highest-level calculations performed, which were used in the kinetics modeling, include optimized geometries of reactants, intermediate species, products and transition states using density functional theory (DFT). Becke's three-parameter hybrid method employing the LYP correlation functional (B3LYP)[27,28] in conjunction with the Pople-style triple-ζ split valence polarized basis sets was used (6-311++G**).[29,30] A schematic energy diagram of the reaction is shown in Figure 4.

The initially activated β-hydroxyalkyl radicals are subject to a competition between collisional stabilization, dissociation, and isomerization. We have employed RRKM theory coupled with the master equation (ME) formalism to calculate reaction rate constants as well as branching ratios among the isomers and into the dissociative channels, to give isoprene and OH or 2-hydroxy-1,3-butadiene and CH_3. Because the OH-isoprene radicals isomerize through well-defined saddle points along the potential energy surface, standard (nonvariational) RRKM theory can be used to calculate microcanonical rate constants as a function of energy. Dissociation to form 2-hydroxy-1,3-butadiene (enol) and CH_3 also takes place through a well-defined transition state. The dissociation of the OH-isoprene adduct to form OH and isoprene, however, takes place on a nearly monotonically increasing potential energy surface. An accurate description of this process requires a two-transition-state model which includes variational treatments of both the inner and the outer transition states. This treatment has been applied to the cases of the hydroxyl radical addition to ethylene and isoprene.[7,8] At high temperatures, the outer transition state becomes unimportant and the kinetic model can be accurately approximated by including only the inner transition state. At 300 K, the inner transition state serves as the dominant bottleneck such that an inclusion of both transition states only reduces the rate by 30%. Furthermore, high level ab initio calculations revealed that the potential energy surface for the adduct dissociation includes a saddle point below the asymptotic energy of separated products and the saddle point appears at carbon−oxygen separation distances near 2.2 Å. For the purposes of this model, a 2.2 Å carbon−oxygen separation was assumed to adequately describe the saddle point for the adduct dissociation channel. A B3LYP/6-311++G** geometry optimization constraining the carbon−oxygen bond distance to 2.2 Å and a corresponding frequency calculation provided harmonic frequencies and rotational constants in order to evaluate the microcanonical number of states for the adduct dissociation channel. The threshold energy was assumed to be the asymptotic energy for separated isoprene and OH. Neglecting variational effects introduces an error of less than 15% to the dissociation rate in the case of ethylene and are, therefore, excluded from the current work.[8]

B3LYP/6-311++G** unscaled vibrational frequencies and rotational constants and energies were used to calculate the RRKM rate constants through the tight transition states. For all species, the density and sum of states were obtained through an exact count procedure by the Stein−Rabinovitch extension[31] of the Beyer−Swinehart algorithm[32] implemented in the MultiWell program suite.[33,34] There was no reaction path degeneracy for the isomerization reactions. The dissociation channels for the isoprene−OH adduct were considered to be irreversible, and the isomerization steps were considered to be reversible. The transformation from the microcanonical rates to thermal rate

constants, and the short-time evolution of the initial OH-isoprene radical distribution, was treated using the one-dimensional, energy grained ME formalism. Implementation of the ME formalism includes activation and deactivation processes as well as unimolecular rate constants for reaction molecules.[35,36] The strong collision approximation is not valid for the treatment of small monatomic or diatomic colliders such as Ar or N_2. A more appropriate treatment includes a weak collision model which has been implemented by applying the exponential down model of energy transfer. We have calculated the collision frequency based on a Lennard-Jones interaction potential. The necessary quantities for the self-collisions of many bath gases (e.g., Ar) and several reactant molecules are listed in the literature.[37] In the case of the hydroxy radicals, it is necessary to estimate ϵ and σ since these are not available. We calculated their values using empirical formulas.[38] The values of $\epsilon = 150.4$ K and $\sigma = 4.9$ Å have been adopted as Lennard-Jones parameters for the interactions between the hydroxyalkyl radicals with Ar.

RRKM/ME calculations were performed at 298 K and 50 Torr in an argon bath gas, to model the chemistry in the laboratory experiments. A Boltzmann distribution, shifted by the exothermicity of the addition reaction, was used for the initial energy distribution of β-hydroxy radicals for the tropospheric simulation.[39] The measured internal energy distribution for the nascent hydroxy radicals from the photodissociation experiment was used as an initial energy distribution to model the laboratory conditions. The RRKM/ME simulations at 50 Torr using a $\Delta E_{down} = 250$ cm^{-1} predicted that 8% of radicals have sufficient internal energy to undergo prompt dissociation to form either isoprene and OH (6%) or spontaneously lose a methyl group to form the corresponding enol (2%). Although the experimentally determined energy distribution is significantly broader than the 298 K Boltzmann distribution, there are several reasons to expect the kinetics to mimic those resulting from the chemical activation of OH addition to isoprene. The highest energy radicals are rapidly lost either to enol formation or OH + isoprene. In addition, we find that there is little difference in the efficiency of forming the more stable α-hydroxyalkyl radical isomer for internal energies near the OH + isoprene asymptote. This is a consequence of isomerization rates which exceed the collisional stabilization rates for these energies. A prompt OH signal, consistent with this dissociation is observed in the LP/LIF experiment and is discussed below. The similarity between the remaining "cooler" radicals and the thermal distribution suggests tropospheric relevance of the ensuing kinetics.

Multiplexed Mass Spectrometry. In order to confirm the reaction mechanism of the β-hydroxyalkyl radicals, formed *via* OH addition to the second position of isoprene, the corresponding iodohydrin was photolyzed in the presence of O_2 and the time-dependences of reaction products were measured using multiplexed photoionization mass spectrometry. Figure 5 illustrates the two possible fates of the β-hydroxyalkyl radicals in the presence of O_2 with the corresponding mass to charge (m/z) ratios observed in the mass spectrometry experiment. Prompt cyclic isomerization of β-hydroxyalkyl radicals ($m/z = 85$), followed by hydrogen abstraction by O_2 yields 4-penten-2-one ($m/z = 84$) and HO_2 ($m/z = 33$), whereas O_2 addition to the β-hydroxyalkyl radicals results in peroxy radicals ($m/z = 117$). The primary m/z ratios of interest in this study are therefore $m/z = 33$, 84, 85, 117, and 127, which correspond to HO_2, 4-penten-2-one, α-and β-hydroxyalkyl radicals, hydroxyalkylperoxy radical, and the iodine atom, respectively. A complete time-dependent mass spectrum of all species is shown in Figure 6 at a VUV energy of 12.0 eV. The figure illustrates the

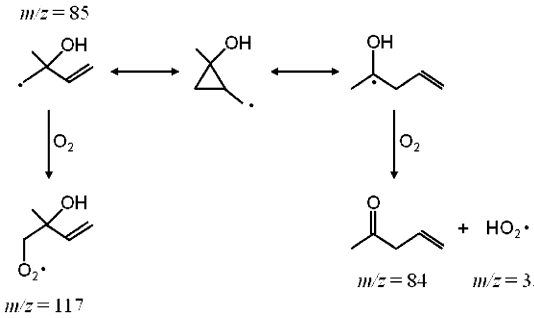

Figure 5. Summary of the reactions of the hydroxyalkyl radicals, isomers II and III, in the presence of O_2 under tropospheric conditions.

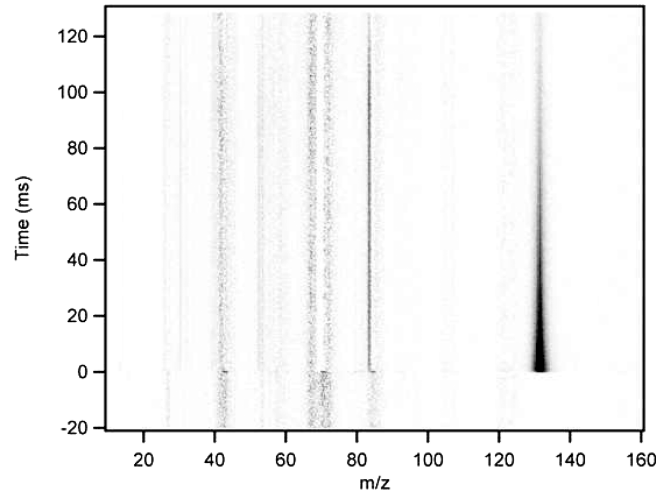

Figure 6. Representative time-resolved mass spectra of the photodissociation of iodohydrin photolytic precursor at 248 nm in the presence of O_2 at 12.0 eV ionization energy.

multiplex advantage of the instrument, i.e., the ability to measure the time dependence of all species simultaneously. Any species observed prior to time zero, defined by the 248 nm photolysis pulse, can be identified as an impurity or the result of dissociative ionization. It is noteworthy that the VUV radiation from the synchrotron light source enables additional chemical species identification by comparison of the measured ionization curves with known standards. In the present experiments the VUV energy was tuned both above and below the ionization energies of the known species, which are HO_2 and iodine atom at 11.35[40] and 10.45[41] eV, respectively. Signal corresponding to the m/z ratios of HO_2, iodine atom, and 4-penten-2-one were observed only at VUV energies above the ionization energies for each species confirming their identity. Although ionization energies and ionization onset curves are not known for all species, careful quantum chemistry calculation with CCSD(T) or QCISD(T) gives very accurate adiabatic ionization energies, with an accuracy of a few hundredths of an electronvolt,[42−45] and less accurate methods like CBS-QB3 still typically return values that are accurate to within about ∼10 kJ mol^{-1} (0.1 eV).[45−47,11] Figure 7 shows the signal as a function of photoionization energy for the $m/z = 84$ species, corresponding to the 4-penten-2-one product. The adiabatic ionization energies for 4-penten-2-one and for other plausible C_5H_8O products were calculated with the CBS-QB3 method[48,26] and are reported in Table 1.

The ionization energies of the enol species that would arise from removal of a hydrogen from a carbon adjacent to the radical site, e.g., by O_2 addition and subsequent HO_2 elimina-

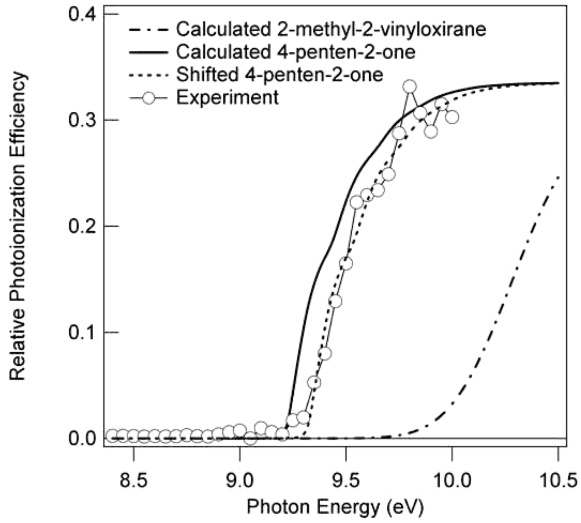

Figure 7. Experimental photoionization efficiency spectrum for the $m/z = 84$ product, compared to calculated photoionization efficiency curves for two possible isomers.

TABLE 1: CBS-QB3 Calculated Ionization Energies for Possible C_5H_8O Products

	adiabatic IE (eV)	vertical IE (eV)[a]
4-penten-2-one	9.24	9.68
2-methyl-2-vinyloxirane	9.19	10.21
1-vinylcyclopropanol	8.43	
2,4-pentadien-2-ol	7.90	
1,4-pentadien-2-ol	8.57	

[a] Relative energy of the cation calculated at the most stable neutral geometry.

tion,[49] lie much lower than the observed onset of the $m/z = 84$ signal. Two conceivable cyclization products of H abstraction (or O_2 addition followed by HO_2 elimination) from the initial β-hydroxyalkyl radical are 1-vinylcyclopropanol and 2-methyl-2-vinyloxirane. Although both of these species also have ionization energies below the experimental onset of $m/z = 84$ signal, the calculated ionization energy of the 2-methyl-2-vinyloxirane is too close to the observed threshold to eliminate that isomer on the basis of IE alone. However, the 2-methyl-2-vinyloxirane undergoes a substantial geometry change upon ionization, resulting in an extended Franck−Condon envelope and a large shift between adiabatic and vertical ionization energies. On the other hand, the 4-penten-2-one isomer has a CBS-QB3 calculated adiabatic ionization energy approximately 0.1 eV below the observed threshold, and a Franck−Condon envelope that closely matches the shape of the observed photoionization efficiency spectrum for the $m/z = 84$ product. Figure 7 also displays computed 300 K spectra for the 4-penten-2-one and 2-methyl-2-vinyloxirane isomers, based on Franck−Condon factors for the photoionization transitions. The Franck−Condon factors are computed using the PESCAL program.[50] The 4-penten-2-one photoionization efficiency spectrum, calculated using the 11 most active vibrational modes, and including Duschinsky rotation,[51] is essentially identical to the observed spectrum if the adiabatic ionization energy is shifted by 0.1 eV from the CBS-QB3 value. The 2-methyl-2-vinyloxirane spectrum, calculated using the four most active modes, is in complete disagreement with the observed spectrum. We note that there are two reports of the product distribution of isoprene oxidation induced by hydroxyl radical in the absence of NO_x.[52,53] In both studies, the authors measured the products using GC/MS and identified a MW = 84 species with the

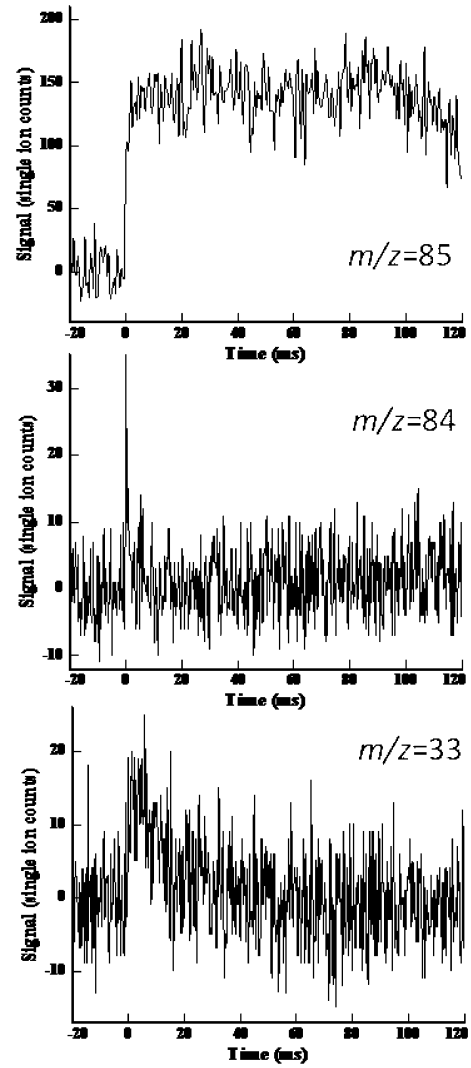

Figure 8. Time-dependent trace of $m/z = 85$ corresponding to the hydroxyalkyl radicals formed upon photolysis of the iodohydrin photolytic precursor (top panel) and $m/z = 84$ (middle panel) taken at a photoionization energy of 9.0 eV. The lower panel shows the time-dependent trace of $m/z = 33$ acquired at a photoionization energy of 12.0 eV corresponding to HO_2.

relative yield of approximately 2%. Although these products were assigned different origins in the two studies, we contend these products are likely 4-penten-2-one and 3-methyl-3-butenal (from OH addition to the other inner carbon position).

Figure 8 shows the time-dependent traces of the hydroxyalkyl radical (top panel), 4-penten-2-one (middle panel), and HO_2 (bottom panel). The plots represent slices (fixed m/z) through the background-subtracted multiplexed data. The hydroxyalkyl radicals ($m/z = 85$) are formed promptly upon photolysis and then rapidly decay within the first few time steps of the experiment, approximately 500 μs. The decay rate of the hydroxyalkyl radical is consistent with the rise times of both 4-penten-2-one and HO_2. The ionization cross section of HO_2 is lower than the 4-penten-2-one resulting in lower absolute signals. The absolute concentration of O_2 was not precisely known during the experiments. Although no O_2 was added to the reaction mixture, minor leaks ensured sufficient O_2 for the hydrogen atom reaction from α-hydroxyalkyl radicals. Kinetic modeling of the decay of the hydroxyalkyl radicals and the rise of 4-peten-2-one, employing the mechanism and rates described in the context of the LP/LIF experiment, suggest an O_2 concentration of approximately 5×10^{14} molecules cm^{-3}. The

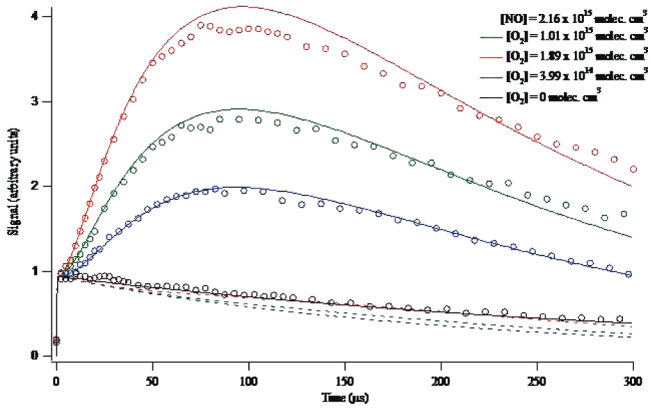

Figure 9. Temporal profiles of OH under two additional constant concentrations of NO with varying O_2 concentrations (symbols) fitted, including the cyclic isomerization pathway (solid lines).

4-penten-2-one product is stable and the measured time trace is constant following the initial rise. The HO_2 trace however exhibits a time-dependent decay due to subsequent reactions. We observed a small time-dependent signal for $m/z = 68$ (isoprene) due to prompt dissociation of the nascent hydroxyalkyl radicals but were unable to detect evidence of enol formation. We also did not observe evidence for the formation of alkyl peroxy radicals at $m/z = 117$ although the detection of these cations is known to be challenging.[11] The appearance of $m/z = 33$ in coincidence with the $m/z = 84$ appearance and the disappearance of $m/z = 85$ is compelling evidence toward a hydrogen abstraction mechanism from α-hydroxyalkyl radicals.

LP/LIF. The LP/LIF studies are similar to those presented in previous work for the case of 1,3-butadiene. In the present case, the temporal profiles of OH are measured following iodohydrin photolysis at 248 nm. All reactions were conducted at room temperature (298 K). A judicious choice of initial conditions and careful sensitivity analysis allows us to model our experimental observations. Figure 9 shows OH temporal profiles under multiple reaction conditions with respect to concentrations of O_2 and NO and overlaid with kinetics fits of the data. OH temporal profiles were followed under conditions including NO in the absence of O_2, and including O_2 in the absence of NO, and in both cases, no rise in OH concentrations were observed. In all cases, the OH signals rise rapidly following the photolysis pulse, increase to a maximum, and subsequently decay. The origin of the rapid rise is the dissociation of metastable nascent β-hydroxyalkyl radicals to give OH and isoprene. The longer rise in OH signal is the result of chemical reactions initiated by isomerization of the β-hydroxyalkyl radicals to α-hydroxyalkyl radicals followed by hydrogen atom abstraction as shown in Figure 5. The decrease in signal at longer times is due to radical sink terms involving NO and the precursor compound. Details regarding the kinetic model are presented below. We note that the measured time-dependent OH concentrations are inconsistent with reaction of β-hydroxyalkyl radicals with O_2 to form peroxy radicals. In fact, any mechanism which neglects the formation of α-hydroxyalkyl radicals fails to reproduce the observed growth of OH under the present experimental NO and O_2 concentrations. The predicted decrease in OH concentration for this mechanism is consistent with previous cycling experiments and is a consequence of loss rates (due to reaction with the iodohydrin precursor) which exceed production rates. Figure 9 demonstrates this point by including fits which exclude the cyclic isomerization (dashed lines).

A numerical program, KINTECUS,[54] was used to simulate the kinetics data and the sensitivity analysis was performed using the same software. The kinetics mechanism, provided in Table 2, involves 29 reactions but is remarkably constrained. Only 7 rate constants, k_1-k_7, were adjusted in the modeling of experimental data. The rate of OH reaction with the iodohydrin precursor was measured employing the LP/LIF technique in our lab yielding a bimolecular rate constant of 1.5×10^{-11} cm^3 s^{-1}. In addition, for several processes only relative branching ratios (not absolute magnitudes) are important due to the rapid time scale not the absolute magnitudes, e.g., k_1-k_4. These ratios reflect the branching of the nascent β-hydroxyalkyl radicals that undergo prompt dissociation to yield either OH + isoprene (k_1) or CH_3 + enol (k_2), isomerize to α-hydroxyalkyl radicals (k_3), or are thermalized (k_4). The kinetic model is very sensitive to the percentage of β-hydroxyalkyl radicals that promptly dissociate to form OH and isoprene. Figure 10 shows a kinetics simulation where 25% of the β-hydroxyalkyl radicals undergo prompt dissociation as compared to the similar simulation including 6% prompt dissociation. The larger value for prompt dissociation limits the total concentration of hydroxyalkyl radicals available to regenerate OH. This is clearly demonstrated by the much smaller rise of OH compared to prompt OH in the simulation including 25% prompt OH dissociation. Therefore our data are consistent with ca. 6% of the nascent β-hydroxyalkyl radicals dissociating to form OH and isoprene. The result is in good agreement with the predictions of RRKM/ME calculations using the initial radical internal energy distribution measured in the VELMI experiments.

Of the surviving nascent β-hydroxyalkyl radicals, another important ratio is k_3/k_4 which is the fraction of cyclic isomerization to form α-hydroxyalkyl radicals to the fraction which collisionally relaxes to form thermalized β-hydroxyalkyl radicals. The fates of the α-hydroxyalkyl radicals are either hydrogen abstraction by O_2 or NO termination. The β-hydroxyalkyl radicals are assumed to follow the conventional hydrocarbon oxidation scheme and either undergo NO termination or O_2 addition. Further reactions of the peroxy radicals resulting from O_2 addition to β-hydroxyalkyl radicals ultimately lead to formation of OH radicals but on a time scale much longer than the observed OH rise in the data. Additional simulations excluding the cyclic isomerization to form α-hydroxyalkyl radicals were inconsistent with the OH temporal profiles.

Sensitivity analysis of the modeling, given the chemical mechanism in Table 2, was also performed. We find that very few of the 28 reactions had high sensitivity coefficients (see the Supporting Information). Based on the model, the hydrogen abstraction rate from the α-hydroxyalkyl radical was determined to be $(3.3 \pm 0.5) \times 10^{-11}$ $cm^3 molecules^{-1} s^{-1}$, where the error reflects 2 standard deviations from the average. Analogous O_2-hydrogen abstraction reactions exhibit similar rate constants. The rate constant for O_2-hydrogen abstraction from the α-hydroxyalkyl radical formed upon cyclic isomerization of the β-hydroxyl alkyl radical in the OH-1,3-butadiene system was experimentally determined to be 3.3×10^{-11} cm^3 $molecules^{-1}$ s^{-1}.[22] Both of those values are within the range of 1.2×10^{-11} to 3.7×10^{-11} cm^3 $molecules^{-1}$ s^{-1} reported by Miyoshi and co-workers[55] for several α-hydroxyalkyl radicals with O_2.We are also able to establish an α/β branching ratio of 7.0 (i.e., 88% of the β-hydroxyalkyl radicals isomerize), which is consistent with the RRKM/ME prediction of 8.6 (i.e., 90% of the β-hydroxyalkyl radicals isomerizes to α-hydroxyalkyl radicals).

Conclusions

We have demonstrated a photolytic route to studying isomer-selective kinetic of OH-initiated oxidation of unsaturated

TABLE 2: Kinetics Mechanism Employed in Modeling the Time-Dependent OH Signals

	reaction	rate constant		ref
k_1	$HOC_5H_8 \rightarrow OH + C_5H_8$	6×10^{10}	s^{-1}	1
k_2	$HOC_5H_8 \rightarrow CH_3 + C_4H_5OH$	2×10^{10}	s^{-1}	*a*
k_3	$HOC_5H_8 \rightarrow \alpha$-$HOC_5H_8$ (isomerization)	8.2×10^{11}	s^{-1}	*a*
k_4	$HOC_5H_8 \rightarrow \beta$-$HOC_5H_8$ (thermalization)	1×10^{11}	s^{-1}	*a*
k_5	α-$HOC_5H_8 + O_2 \rightarrow \alpha$-$C_5H_8O+HO_2$	$(3.3 \pm 0.5) \times 10^{-11}$	cm^3 molec.$^{-1}$ s^{-1}	*b*, 55
k_6	α-$HOC_5H_8 + NO \rightarrow \alpha$-$HOC_5H_8NO$	$(2.8 \pm 0.6) \times 10^{-11}$	cm^3 molec.$^{-1}$ s^{-1}	*b*, 56, 57
k_7	β-$HOC_5H_8 + NO \rightarrow \beta$-$HOC_5H_8NO$	$(2.8 \pm 0.6) \times 10^{-11}$	cm^3 molec.$^{-1}$ s^{-1}	*b*, 56, 57
k_8	β-$HOC_5H_8 + O_2 \rightarrow \beta$-$HOC_5H_8O_2$	2.3×10^{-12}	cm^3 molec.$^{-1}$ s^{-1}	56, 58
k_9	β-$HOC_5H_8O_2 + NO \rightarrow \beta$-$HOC_5H_8O + NO_2$	8.5×10^{-12}	cm^3 molec.$^{-1}$ s^{-1}	59, 60
k_{10}	β-$HOC_5H_8O_2 + NO \rightarrow \beta$-$HOC_5H_8ONO_2$	4.5×10^{-13}	cm^3 molec.$^{-1}$ s^{-1}	59, 60
k_{11}	β-$HOC_5H_8O \rightarrow CH_2O + HOC_4H_6$	5×10^5	s^{-1}	61
k_{12}	β-$HOC_5H_8O + NO \rightarrow \beta$-$HOC_5H_8ONO$	3×10^{-11}	cm^3 molec.$^{-1}$ s^{-1}	56, 57, 62
k_{13}	$HOC_4H_6 + O_2 \rightarrow C_4H_6O + HO_2$	3×10^{-11}	cm^3 molec.$^{-1}$ s^{-1}	55
k_{14}	$HOC_4H_6 + NO \rightarrow HOC_4H_6NO$	3×10^{-11}	cm^3 molec.$^{-1}$ s^{-1}	56, 57
k_{15}	$HO_2 + NO \rightarrow OH + NO_2$	8.8×10^{-12}	cm^3 molec.$^{-1}$ s^{-1}	60, 63
k_{16}	$HO_2 + NO_2 \rightarrow HO_2NO_2$	2.23×10^{-13}	cm^3 molec.$^{-1}$ s^{-1}	60, 63
k_{17}	$HO_2 + HO_2 \rightarrow H_2O_2 + O_2$	1.6×10^{-12}	cm^3 molec.$^{-1}$ s^{-1}	60, 63
k_{18}	$OH + NO \rightarrow HONO$	9.4×10^{-13}	cm^3 molec.$^{-1}$ s^{-1}	60
k_{19}	$OH + NO_2 \rightarrow HONO_2$	2.22×10^{-12}	cm^3 molec.$^{-1}$ s^{-1}	60
k_{20}	$OH + NO_2 \rightarrow HO_2 + NO$	5.34×10^{-14}	cm^3 molec.$^{-1}$ s^{-1}	60
k_{21}	$OH + OH \rightarrow H_2O_2$	8.97×10^{-13}	cm^3 molec.$^{-1}$ s^{-1}	64
k_{22}	$OH + OH \rightarrow H_2O + O$	1.48×10^{-12}	cm^3 molec.$^{-1}$ s^{-1}	64
k_{23}	$OH + HO_2 \rightarrow O_2 + H_2O$	1.1×10^{-10}	cm^3 molec.$^{-1}$ s^{-1}	64
k_{24}	$OH + H_2O_2 \rightarrow H_2O + HO_2$	1.7×10^{-12}	cm^3 molec.$^{-1}$ s^{-1}	64
k_{25}	$OH + HONO \rightarrow H_2O + NO_2$	6×10^{-12}	cm^3 molec.$^{-1}$ s^{-1}	64
k_{26}	$OH + HO_2NO_2 \rightarrow$ products	4.7×10^{-12}	cm^3 molec.$^{-1}$ s^{-1}	64
k_{27}	$OH + HONO_2 \rightarrow H_2O + NO_3$	1.5×10^{-13}	cm^3 molec.$^{-1}$ s^{-1}	64
k_{28}	$OH + IHOC_5H_8 \rightarrow IHOC_5H_8OH$	1.5×10^{-11}	cm^3 molec.$^{-1}$ s^{-1}	*c*
k_{29}	$OH + C_5H_8 \rightarrow HOC_5H_8$	1×10^{-10}	cm^3 molec.$^{-1}$ s^{-1}	22

[a] RRKM/ME simulations. [b] Adjusted for best fit. [c] This work.

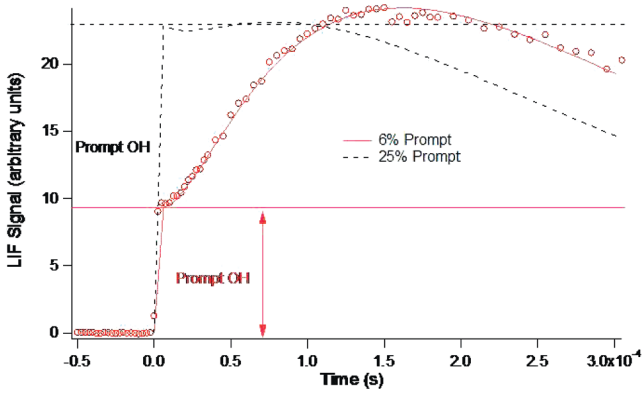

Figure 10. Temporal profiles of OH (symbols) fitted, considering considering 6% and 25% prompt OH formation due to dissociation of hot β-hydroxyalkyl radicals (solid and dashed lines, respectively).

hydrocarbons using the UV photolysis of iodohydrins. Velocity map ion imaging permits the direct determination of the internal energy distribution of the nascent radical ensuring that the energy distribution of the radicals can be "tuned" to mimic the radicals formed from electrophilic−OH addition. The present study focuses on the reactivity of the nascent β-hydroxyalkyl radicals formed when isoprene undergoes oxidation by hydroxyl radical addition to the inner carbons. We have confirmed the "new" chemistry of these species, namely a cyclic isomerization pathway to yield α-hydroxy radicals which undergo reaction with O_2 to form C_5-carbonyls. The combination of time-resolved multiplexed photoionization mass spectrometry and LP/LIF studies provides compelling evidence for the cyclic isomerization pathway through the measurement of the time-dependent behavior of the relevant species. The time-dependence of OH generation during the LP/LIF kinetics experiments supports the cyclic isomerization mechanism to α-hydroxyalkyl radicals and also provides a hydrogen abstraction rate constant for O_2 reaction with the α-hydroxyalkyl radical of $(3.3 \pm 0.5) \times 10^{-11}$ cm^3 molecule^{-1} s^{-1}.

Acknowledgment. This work was supported by the National Science Foundation (Grant No. CHE-0204705), the Environmental Protection Agency (Grant No. R03-0132), the Robert A. Welch Foundation (A-1405), and the Texas Advanced Research Program (Grant No. 010366-0306). The participation of F.G. was supported by the National Aeronautics and Space Administration (NASA, Grant NAGS-13339). The Advanced Light Source is supported by the Director, Office of Science, Office of Basic Energy Sciences, Materials Sciences Division, of the U.S. Department of Energy under Contract No. DE-AC02-05CH11231 at Lawrence Berkeley National Laboratory. The work of P.Z., T.M.S., D.L.O., G.M., and C.A.T. was supported by the Division of Chemical Sciences, Geosciences, and Biosciences, the Office of Basic Energy Sciences, the U.S. Department of Energy. Sandia is a multiprogram laboratory operated by Sandia Corporation, a Lockheed Martin Company, for the National Nuclear Security Administration under Contract DE-AC04-94-AL85000.

Supporting Information Available: ^{1}H NMR and a UV−vis spectrum. This material is available free of charge via the Internet at http://pubs.acs.org.

References and Notes

(1) Atkinson, R. Gas-Phase Tropospheric Chemistry of Organic Compounds. *J. Phys. Chem. Ref. Data Monogr.* **1994**, *2*, 1.

(2) Seinfeld, J. H.; Pandis, S. N. *Atmospheric Chemistry and Physics: From Air Pollution to Climate Change*; John Wiley & Sons, Inc.: New York, 1997.

(3) IPCC Scientific Assessment, Climate Change; Cambridge University Press: New York, 1992.

(4) Chameides, W. L.; Fehsenfeld, F.; Rodgers, M. O.; Cardelino, C.; Martinez, J.; Parrish, D.; Lonneman, W.; Lawson, D. R.; Rasmussen, R. A.; Zimmerman, P.; Greenberg, J.; Middleton, P.; Wang, T. Ozone Precursor Relationships in the Ambient Atmosphere. *J. Geophys. Res. [Atmospheres]* **1992**, *97*, 6037–6055.

(5) Rasmussen, R. A.; Khalil, M. A. K. Isoprene over the Amazon Basin. *J. Geophys. Res. [Atmospheres]* **1988**, *93*, 1417–1421.

(6) Claeys, M.; Graham, B.; Vas, G.; Wang, W.; Vermeylen, R.; Pashynska, V.; Cafmeyer, J.; Guyon, P.; Andreae, M. O.; Artaxo, P.; Maenhaut, W. Formation of Secondary Organic Aerosols Through Photooxidation of Isoprene. *Science* **2004**, *303*, 1173–1176.

(7) Greenwald, E. E.; North, S. W.; Georgievskii, Y.; Klippenstein, S. J. *J. Phys. Chem. A* **2007**, *111*, 5582.

(8) Greenwald, E. E.; North, S. W.; Georgievskii, Y.; Klippenstein, S. J. *J. Phys. Chem. A* **2005**, *109*, 6031.

(9) Zou, P.; Kim, H.; North, S. W. *J. Chem. Phys.* **2002**, *116*, 4176. Kim, H.; Park, J.; Niday, T. C.; North, S. W. *J. Chem. Phys.* **2005**, *123*, 174303. Eppink, A. T. J. B.; Parker, D. H. *Rev. Sci. Instrum.* **1997**, *68*, 3477.

(10) Osborn, D. L.; Zou, P.; Johnsen, H.; Hayden, C. C.; Taatjes, C. A.; Knyazev, V. D.; North, S. W.; Peterka, D. S.; Ahmed, M.; Leone, S. R. *Rev. Sci. Instrum.* **2008**, *79*, 10410.

(11) Meloni, G.; Zou, P.; Klippenstein, S. J.; Ahmed, M.; Leone, S. R.; Taatjes, C. A.; Osborn, D. L. *J. Am. Chem. Soc.* **2006**, *128*, 13559.

(12) Goulay, F.; Osborn, D. L.; Taatjes, C. A.; Zou, P.; Meloni, G.; Leone, S. R. *Phys. Chem. Chem. Phys.* **2007**, *9*, 4291.

(13) Taatjes, C. A.; Hansen, N.; Osborn, D. L.; Kohse-Höinghaus, K.; Cool, T. A.; Westmoreland, P. R. *Phys. Chem. Chem. Phys.* **2008**, *10*, 20.

(14) McGivern, W. S.; Suh, I. S.; Clinkenbeard, A. D.; Zhang, R.; North, S. W. *J. Phys. Chem. A* **2000**, *104*, 6609. Reitz, J. E.; McGivern, W. S.; Church, M. C.; Wilson, M. D.; North, S. W. *Int. J. Chem. Kinet.* **2002**, *34*, 255.

(15) Barluenga, J.; Marco-Arias, M.; González-Bobes, F.; Ballesteros, A.; González, J. M. *Chem.—Eur. J.* **2004**, *10*, 1677.

(16) It was found that diluting 33 mL of 18 M sulfuric acid with half of the prescribed distilled water (solvent) to produce 83 mL of 7.2 M sulfuric acid was preferable as predissociation followed by cooling of the acid reduced the amount of heat added to the reaction solution.

(17) Additionally, the hexanes were difficult to remove completely from the final product. It is speculated that the THF, which is difficult to entirely remove from the sample, created challenges during the column chromatography step.

(18) It is worth noting that some heat during the distillation steps would have increased the removal of THF and hexanes. However, the product is not well characterized, and based on the darkening of the product (to a deep red) upon heating, we were concerned that, though we may have been completely removing organic impurities obtained during the synthesis, we were degrading our product and forming polymer impurities.

(19) Garcia, G. A.; Nahon, L.; Powis, I. *Rev. Sci. Instrum.* **2004**, *75*, 4989.

(20) Zare, R. N. *Mol. Photochem.* **1972**, *4*, 1.

(21) Hess, W. P.; Kohler, S. J.; Haugen, H. K.; Leone, S. R. *J. Chem. Phys.* **1986**, *84*, 2143.

(22) Greenwald, E. E.; Anderson, K. C.; Park, J.; Kim, H.; Reich, B. J. E.; Miller, S. A.; North, S. W. *J. Phys. Chem. A* **2005**, *109*, 7915.

(23) Krajnovich, D.; Butler, L. J.; Lee, Y. T. *J. Chem. Phys.* **1984**, *81*, 3031. (a) Minton, T. K.; Felder, P.; Brudzynski, R. J.; Lee, Y. T. *J. Chem. Phys.* **1984**, *81*, 1759. Minton, T. K.; Nathanson, G. M.; Lee, Y. T. *J. Chem. Phys.* **1987**, *86*, 1991.

(24) Calculated at the B3LYP level of theory, as implemented in Gaussian03 rev. E.01, with the cc-pVQZ basis set on C, O, and H, and the cc-pVQZ-PP basis set with a small core ECP on I.

(25) Park, J.; Jongsma, C. G.; Zhang, R.; North, S. W. *Phys. Chem. Chem. Phys.* **2003**, *5*, 3638.

(26) Frisch, M. J.; Trucks, G. W.; Schlegel, H. B.; Scuseria, G. E.; Robb, M. A.; Cheeseman, J. R.; Montgomery, J. A., Jr.; Vreven, T.; Kudin, K. N.; Burant, J. C.; Millam, J. M.; Iyengar, S. S.; Tomasi, J.; Barone, V.; Mennucci, B.; Cossi, M.; Scalmani, G.; Rega, N.; Petersson, G. A.; Nakatsuji, H.; Hada, M.; Ehara, M.; Toyota, K.; Fukuda, R.; Hasegawa, J.; Ishida, M.; Nakajima, T.; Honda, Y.; Kitao, O.; Nakai, H.; Klene, M.; Li, X.; Knox, J. E.; Hratchian, H. P.; Cross, J. B.; Bakken, V.; Adamo, C.; Jaramillo, J.; Gomperts, R.; Stratmann, R. E.; Yazyev, O.; Austin, A. J.; Cammi, R.; Pomelli, C.; Ochterski, J. W.; Ayala, P. Y.; Morokuma, K.; Voth, G. A.; Salvador, P.; Dannenberg, J. J.; Zakrzewski, V. G.; Dapprich, S.; Daniels, A. D.; Strain, M. C.; Farkas, O.; Malick, D. K.; Rabuck, A. D.; Raghavachari, K.; Foresman, J. B.; Ortiz, J. V.; Cui, Q.; Baboul, A. G.; Clifford, S.; Cioslowski, J.; Stefanov, B. B.; Liu, G.; Liashenko, A.; Piskorz, P.; Komaromi, I.; Martin, R. L.; Fox, D. J.; Keith, T.; Al-Laham, M. A.; Peng, C. Y.; Nanayakkara, A.; Challacombe, M.; Gill, P. M. W.; Johnson, B.; Chen, W.; Wong, M. W.; Gonzalez, C.; Pople, J. A. Gaussian 03, revision C.02; Gaussian, Inc.: Wallingford, CT, 2004.

(27) Becke, A. D. *J. Chem. Phys.* **1993**, *98*, 5648.

(28) Lee, C.; Yang, W.; Parr, R. G. *Phys. Rev. B* **1988**, *37*, 785.

(29) McLean, A. D.; Chandler, G. S. *J. Chem. Phys.* **1980**, *72*, 5639.

(30) Krishnan, R.; Binkley, J. S.; Seeger, R.; Pople, J. A. *J. Chem. Phys.* **1980**, *72*, 650.

(31) Stein, S. E.; Ravinovitch, B. S. *J. Chem. Phys.* **1973**, *58*, 2438.

(32) Beyer, T.; Swinehart, D. R. *ACM Commun.* **1973**, *16*, 379.

(33) Barker, J. R. *MultiWell Software Ver. 1.3.1*; http://aoss.engin.umich.edu/multiwell/, Ann Arbor, MI, 2002.

(34) Barker, J. R. *Int. J. Chem. Kinet.* **2001**, *33*, 232.

(35) See ref 33.

(36) Barker, J. R. *Int. J. Chem. Kinet.* **2001**, *33*, 232.

(37) Gilbert, R. G.; Smith, S. C. *Theory of Unimolecular and Recombination Reactions* Blackwell: Oxford, 1990.

(38) See ref 37.

(39) A Boltzmann internal energy distribution for the OH-isoprene adduct was calculated, including vibrational and rotational contributions to the density of states, and then offset by the association energy of hydroxyl radical and isoprene (19.5 kcal/mol), which includes zero-point energy.

(40) Dyke, J. M.; Jonathan, N. B. H.; Morris, A.; Winter, M. *Mol. Phys.* **1981**, *44*, 1059. as presented on webbook.nist.gov.

(41) Lide, D. R., Ed.; *Handbook of Chemistry and Physics*; CRC Press: Boca Raton, FL, 1992; pp 10−211 (as presented on webbook.nist.gov).

(42) Hansen, N.; Klippenstein, S. J.; Westmoreland, P. R.; Kasper, T.; Kohse-Höinghaus, K.; Wang, J.; Cool, T. A. *Phys. Chem. Chem. Phys.* **2008**, *10*, 366.

(43) Taatjes, C. A.; Klippenstein, S. J.; Hansen, N.; Miller, J. A.; Cool, T. A.; Wang, J.; Law, M. E.; Westmoreland, P. R. *Phys. Chem. Chem. Phys.* **2005**, *7*, 806.

(44) Lau, K.-C.; Ng, C.-Y. *Acc. Chem. Res.* **2006**, *39*, 823.

(45) Taatjes, C. A.; Meloni, G.; Selby, T. M.; Trevitt, A. J.; Osborn, D. L.; Percival, C. J.; Shallcross, D. E. *J. Am. Chem. Soc.* **2008**, *130*, 11883.

(46) Meloni, G.; Selby, T. M.; Goulay, F.; Leone, S. R.; Osborn, D. L.; Taatjes, C. A. *J. Am. Chem. Soc.* **2007**, *129*, 14019.

(47) Meloni, G.; Selby, T. M.; Osborn, D. L.; Taatjes, C. A. *J. Phys. Chem. A* **2008**, *112*, 13444.

(48) Montgomery, J. A.; Frisch, M. J.; Ochterski, J. W.; Petersson, G. A. *J. Chem. Phys.* **1999**, *110*, 2822.

(49) Zádor, J.; Fernandes, R. X.; Georgievskii, Y.; Meloni, G.; Taatjes, C. A.; Miller, J. A. *Proc. Combust. Inst.* **2009**, *32*, 271.

(50) Ervin, K. M. PESCAL, Fortran program. 2009.

(51) Duschinsky, F. *Acta Physicochim. URSS* **1937**, *7*, 551.

(52) Belkelberg, H.-J.; Böge, O.; Seuwen, R.; Warneck, P. *Phys. Chem. Chem. Phys.* **2000**, *2*, 4029.

(53) Yu, J.; Jeffries, H.; Le, R. M.; Lacheur, Le *Environ. Sci. Technol.* **1995**, *29*, 1923.

(54) Ianni, J. C. Kintecus Windows Version 2.80, **2002**, www.kintecus.com.

(55) Miyoshi, A.; Matsui, H.; Washida, N. *J. Phys. Chem.* **1990**, *94*, 3016.

(56) Atkinson, R. *J. Phys. Chem. Ref. Data* **1997**, *26*, 215.

(57) Lotz, Ch.; Zellner, R. *Phys. Chem. Chem. Phys.* **2001**, *3*, 2607. Deng, W.; Wang, C.; Katz, Dr. R.; Gawinski, G. R.; Davis, A. J.; Dibble, T. S. *Chem. Phys. Lett.* **2000**, *330*, 541. Blitz, M.; Pilling, M. J.; Robertson, S. H.; Seakins, P. W. *Phys. Chem. Chem. Phys.* **1999**, *1*, 73.

(58) Park, J.; Jongsma, C. G.; Zhang, R.; North, S. W. *J. Phys. Chem. A* **2004**, *108*, 10688.

(59) Reitz, J. E.; McGivern, W. S.; Church, M. C.; Wilson, M. D.; North, S. W. *Int. J. Chem. Kinet.* **2002**, *34*, 255. Zhang, D.; Zhang, R.; North, S. W. *J. Phys. Chem. A* **2003**, *107*, 11013.

(60) Sander, S. P.; Freidl, R. R.; Golden, D. M.; Kurylo, M. J.; Huie, R. E.; Orkin, V. L.; Moortgat, G. K.; Ravishankara, A. R.; Kolb, C. E.; Molina, M. J.; Finlayson-Pitts, B. J. *Chemical Kinetics and Photochemical Data for Use in Stratospheric Modeling. JPL Publ. 02−25*; Jet Propulsion Lab: Pasadena, CA, 2003. Eberhard, J.; Howard, C. J. *Int. J. Chem. Kinet.* **1996**, *28*, 731. Becker, K. H.; Geiger, H.; Weisen, P. *Chem. Phys. Lett.* **1991**, *184*, 256.

(61) Park, J.; Stephens, J. C.; Zhang, R.; North, S. W. *J. Phys. Chem. A* **2003**, *107*, 6408.

(62) Falgayrac, G.; Caralp, F.; Sokolowski-Gomex, N.; Devolder, P.; Fittschen, C. *Phys. Chem. Chem. Phys.* **2004**, *6*, 4127.

(63) Atkinson, R.; Baulch, D. L.; Cox, R. A.; Crowley, J. N.; Hampson, R. F., Jr.; Kerr, J. A.; Rossi, M. J.; Troe, J. Summary of Evaluated Kinetic and Photochemical Data for Atmospheric Chemistry. *IUPAC Subcommittee on Gas Kinetic Data Evaluation for Atmospheric Chemistry*; Blackwell: London, 2002.

(64) Atkinson, R.; Baulch, D. L.; Cox, R. A.; Crowley, J. N.; Hampson, R. F.; Hynes, R. G.; Jenkin, M. E.; Rossi, M. J.; Troe, J. *Atmos. Chem. Phys.* **2004**, *4*, 1461.

JP908543A